Nuclear Inst. and Methods in Physics Research, A 928 (2019) 7–12

Contents lists available at ScienceDirect

Nuclear Inst. and Methods in Physics Research, A

journal homepage: www.elsevier.com/locate/nima

A Multigap Resistive Plate Chamber built with thin low-resistive glass: High rate capability with excellent time resolution

Z. Liu [a,b,*], M.C.S. Williams [a,c,d], A. Zichichi [a,d,e], R. Zuyeuski [b,e]

[a] European Centre for Nuclear Research (CERN), Geneva, Switzerland
[b] ICSC World Laboratory, Geneva, Switzerland
[c] Gangneung-Wonju National University, Gangneung, South Korea
[d] INFN and Dipartimento di Fisica e Astronomia, Universit di Bologna, Italy
[e] Museo Storico della Fisica e Centro Studi e Ricerche E.Fermi, Roma, Italy

ARTICLE INFO

Keywords:
Multigap Resistive Plate Chamber
Low-resistive glass
Rate capability
Efficiency
Time resolution

ABSTRACT

Two Multigap Resistive Plate Chambers (MRPCs) were built with thin (0.4 mm) low-resistive glass sheets for the inner plates and standard 0.28 mm 'soda lime' float glass as external plates. The 6-gap MRPC reaches 96.5% efficiency at 15.6 kV and a time resolution of 68 ps at an instantaneous particle flux around 2.5 kHz/cm^2. The 20-gap MRPC reaches 98% efficiency at 18.8 kV and a time resolution of 32 ps. Compared to a 6-gap MRPC built previously with all plates made with soda-lime float glass, the two MRPCs made with low-resistive inner glass show a much higher count rate capability. A third MRPC with all plates made from low-resistive glass was also constructed to verify the operation at high particle flux. In this paper a relative rate capability comparison between the MRPCs has been performed under a pulsed beam with a small spot on the chamber. Their rate capability under full illumination with continuous particle flux needs to be further studied.

1. Introduction

The excellent timing performance of Multigap Resistive Plate Chamber (MRPC) makes it widely used in high energy physics and nuclear experiments. In the last decade, MRPCs have been successfully operated as time of flight (TOF) detectors in the ALICE experiment [1], the HADES experiment [2] and the STAR experiment [3]. Most MRPCs are used in experiments that need a rate capability of charged particle flux below 1 kHz/cm^2; thus 'soda lime' glass ($\rho = 5\times10^{12}$ Ω cm) can be used. The Compressed Baryonic Matter (CBM) experiment is being planned at the Facility for Antiproton and Ion Research (FAIR) to study nucleus–nucleus collisions [4]. As the candidate for CBM TOF system, MRPCs are required to work at particle fluxes in the order of 1–10 kHz/cm^2 for the outer region and 10–25 kHz/cm^2 for the central region [5]. Thus the rate capability will be a key point for the MRPCs used at the CBM experiment. Increasing the temperature of MRPC is a way to improve the rate capability but the dark count rate also increases [6]. Additionally, it is difficult to keep such a large piece of equipment at a stable high temperature for a long period of time; it would increase the cost and the complexity. It has also been shown that the rate capability of MRPC can be improved by using lower resistive materials [7,8]. However, the thickness of low-resistive materials is often thicker (more than 0.7 mm) than the commercial soda-lime float glass (0.28 mm for instance). We have received new low-resistive glass samples[1] with 0.4 mm thickness, which is commercially available. It should be noted that this glass is manufactured by industry using standard high volume production techniques and has a bulk resistivity of 2.1×10^{10} Ω cm at 24 °C (3.8×10^{10} Ω cm at 21 °C) measured by our group. We have first constructed two MRPCs by using these low-resistive glass sheets just for the inner plates to check if it works well for MRPCs and maintains the good performance. We found that this low-resistive glass operated correctly and led to an increase of the rate capability compared to MRPCs built with soda-lime float glass. Finally, another 6-gap MRPC fully equipped with the low-resistive glass has also been tested. It demonstrates a very high rate capability and good performance as expected.

2. MRPC construction

Four MRPCs have been constructed. Three of them have a single-stack geometry. For the single stack MRPCs, the stack is formed as 6 gas gaps with 2 outer glass plates and 5 inner glass plates. They are built with the same read out configuration for direct comparison. Two different glass sheets are used for our MRPC study. One is the soda-lime float glass sheet of 0.28 mm thickness with a bulk resistivity of

* Corresponding author at: European Centre for Nuclear Research (CERN), Geneva, Switzerland.
E-mail address: zheng.liu@cern.ch (Z. Liu).

[1] The samples are received from Picotech SAS.

https://doi.org/10.1016/j.nima.2019.03.016
Received 26 October 2018; Received in revised form 18 January 2019; Accepted 6 March 2019
Available online 8 March 2019

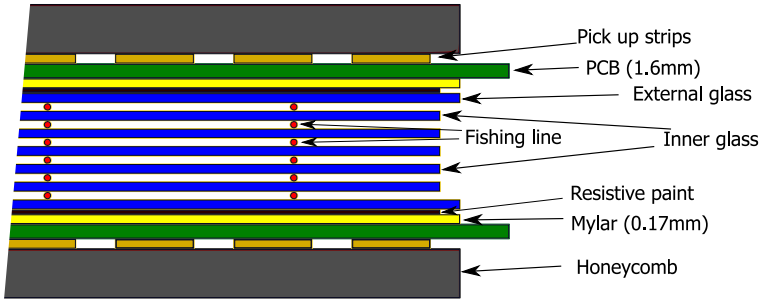

Fig. 1. Cross section view of the 6-gap MRPC with 0.22 mm gas gaps.

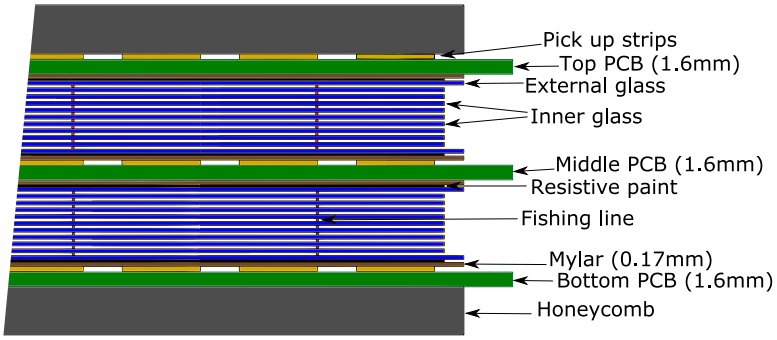

Fig. 2. Cross section view of the low resistivity 20-gap MRPC with 0.16 mm gas gaps.

1.3×10^{12} Ω cm at 24 °C (1.9×10^{12} Ω cm at 21 °C) and the other is the 0.4 mm thickness low-resistive glass sheet with a bulk resistivity of 2.1×10^{10} Ω cm at 24 °C (3.8×10^{10} Ω cm at 21 °C). The first 6-gap MRPC (we will refer to this MRPC as the 'normal 6-gap MRPC') is with all resistive plates made from soda-lime float glass (0.28 mm thickness). Its active area is 18×18 cm^2. The second 6-gap MRPC (we will refer to this MRPC as the 'inner low-resistivity 6-gap MRPC' in the following) uses five low-resistive glass sheets for the inner plates and two soda-lime float glass sheets for the external plates. It also has an active area of 18×18 cm^2. The third 6-gap MRPC (we will refer to this MRPC as the 'all low-resistivity 6-gap MRPC' in the following) low-resistive glass sheets for both inner and external plates. It has a smaller active area of 5×6 cm^2, which is close to the T10 beam spot area. The outer surface of the external glass sheets was coated with resistive material to form a resistive electrode with a surface resistivity of 5 MΩ/□. As shown in Fig. 1, the resistive coating has a gap of 1 cm to the edge of the external glass to prevent high voltage breakdown. Fishing line, with a diameter of 220 μm, was used to form a 220 μm gap size between the glass plates. A mylar sheet was placed between the resistive electrode and the printed circuit board (PCB) to isolate the high voltage. The MRPCs are read out by strips on the top and bottom PCBs. The width of the readout strip is 0.7 cm and the pitch is 0.9 cm.

As we have reported previously in [9], reducing the gap size can also improve the rate capability of MRPC together with the advantage of excellent timing performance. The inner glass of this MRPC (we will refer to this MRPC as the 'low-resistivity 20-gap MRPC' in the following) is as similar construction as low-resistivity 6-gap MRPC. The external glass sheets are the 0.28 mm thickness soda-lime float glass sheets, while the inner plates are 400 μm thick low-resistivity glass sheets. As shown in Fig. 2, it has a similar configuration to a 20 gap chamber previously tested [9]. Each stack was made with 2 outer glass plates and 9 inner glass plates with a gap size of 160 μm. The two resistive electrodes near the middle PCB were connected with negative high voltage and the other two electrodes on the top and bottom layer connected to positive high voltage. Thus this MRPC has two anode readout electrodes (top and bottom) and one cathode readout electrode (middle). The width of the readout strip is 1 cm and the pitch is 1.2 cm. The length of the strips is 21 cm.

All four MRPCs are supported by honeycomb and closed inside a gas tight aluminium box.

3. Experiment setup

We have tested these MRPCs in the T10 beam facility at CERN [10] with a room temperature of 21 °C. A drawing of the experimental setup is shown in Fig. 3. The beam (mostly negative pions of 5 GeV/c momentum) had a direction perpendicular to the chambers. All chambers were flushed with a gas mixture of 95% $C_2H_2F_4$ and 5% SF_6. The crossing of two scintillators of set 1 (P1, P2) defines an area of 1.2×1.2 cm^2 and set 2 (P3, P4) defines 1.9×1.9 cm^2. The scintillators of two sets are read out by photomultiplier tubes (PMTs). Scintillator set 3 consists of two orthogonal scintillator bars with a dimension of $2 \times 2 \times 20$ cm^3. Each end of each bar is coupled to a PMT (S1 and S2 for one bar, S3 and S4 for the other bar). The signals from these four PMTs are discriminated by a constant fraction discriminator. In our measurement, the reference time given by the four PMTs ($(t_{S1} + t_{S2} + t_{S3} + t_{S4})/4$) has a time resolution of 35.0 ± 0.7 ps. All three sets were well aligned with respect to the beam line and defined a small (1.2×1.2 cm^2) area of the beam to provide the trigger signal. The beam spill has a duration of 360 ms. By measuring the number of coincidences of set 1 and set 2 during the spill we can monitor the instantaneous flux of particles that go through the MRPCs. By setting the magnet parameters of T10 beam, we focused the beam to a cross section of 13 mm × 35 mm. Fig. 4 shows the beam profile measured by the wire chamber in both the vertical axis and the horizontal axis at the flux of 25 kHz/cm^2. As seen from the wire chamber profile, a small area (1.3 cm × 3.5 cm) of MRPC is under uniform particles illumination during the period of the beam spill. The MRPC was aligned with beam line so that the beam was

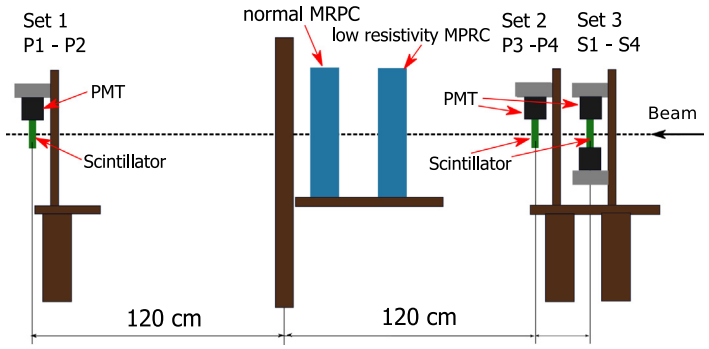

Fig. 3. The experiment setup for MRPC test in T10 test beam facility.

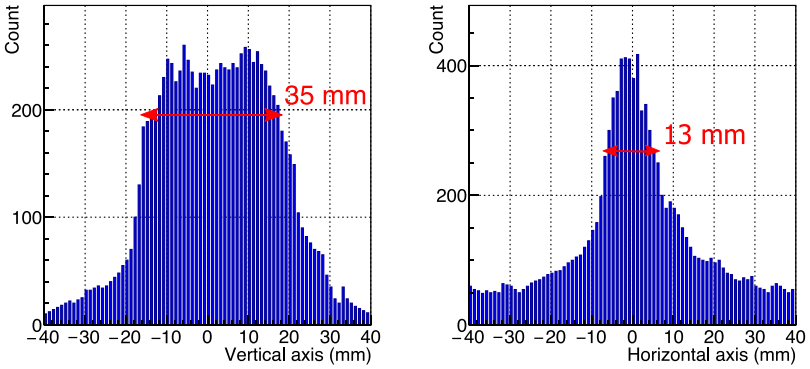

Fig. 4. The wire chamber profile in vertical and horizontal axis at the flux of 25 kHz/cm^2.

centred in the middle of one pick up strip of the MRPC. The signals from the MRPC are discriminated by the NINO ASIC [11]. The output pulse from NINO ASIC is sent to a LVDS-to-NIM converter and readout by WaveCatcher [12]. The WaveCatcher opened an acquisition window when the trigger from the PMTs logic signals are valid. Then the logic signal after the discriminator from the MRPC and time reference PMTs are then sampled and the time of their rising edges and falling edges are recorded.

4. Results

4.1. High voltage scan of MRPCs

All results here are from T10, which has a pulsed beam with a small beam spot focused on the chamber. The MRPC flux is monitored from the count rates of the scintillator sets within the 360 ms duration of the spill. Thus the comparative performance of various MRPCs can be examined — but the performance for a continuous flux of particles over the full area of the chamber is difficult to evaluate.

The four MRPCs have been first tested at a low flux of 2.5 kHz/cm^2. In our analysis, if all 4 timing PMTs register a valid time, this event is regarded as a valid event. If any channel of the MRPC within certain timing window is recorded with a time-over-threshold (ToT) larger than 8 ns, this is recognised as a MRPC hit. The efficiency of the MRPC is calculated as Efficiency = (Total MRPC hits)/(Total valid events). The efficiency of four MRPCs at different electric fields is shown in Fig. 5. The maximum efficiency of these three MRPCs is around 96.5% on their efficiency plateau. However, the electric field at the start point of their plateaux is different. The all low-resistivity 6-gap MRPC reaches the plateau at lowest electric field and the normal 6-gap MRPC reaches its plateau at highest electric field. This higher electric field needed for the normal 6-gap MRPC is caused by the voltage drop across the resistive plates caused by the charge created by avalanches initiated by through-going charge particles. The efficiency of inner low-resistivity 20-gap MRPC reaches a plateau at 115.0 kV/cm with a value of 98.3%.

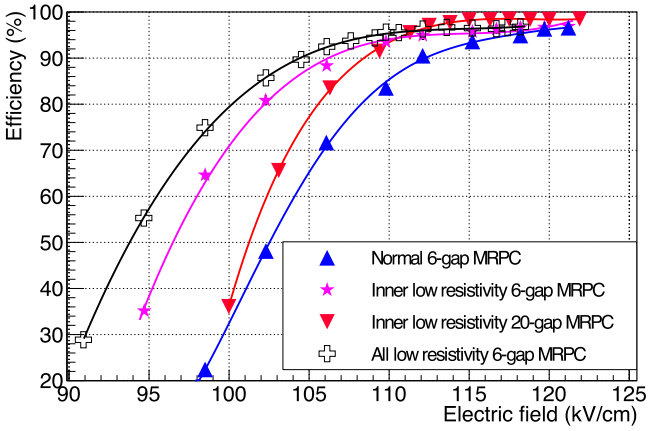

Fig. 5. The efficiency of the four MRPCs as a function at different electric fields at a particle flux of 2.5 kHz/cm^2. The error bars are contained in the size of the symbols; the lines are just to guide the eye.

The dark current of the total active area of the two 6 gas gaps MRPCs is below 40 nA when the electric field is below 121.2 kV/cm. For the same active area the dark current of inner low-resistivity 20-gap MRPC is below 50 nA when the electric field is below 120.0 kV/cm.

The time of the hit in the MRPC was determined from the average time recorded at each end of the strip, thus the MRPC time is independent of the position of the hit. There is a time slewing dependent on the input signal amplitude since NINO chip is set at a fixed threshold for MRPC signal discrimination. A slewing correction is calculated using the pulse width (ToT) information. The detail of the slewing correction procedure can be found in [9]. For our time measurement for the strip, only the single hit event is considered. An example of the ToT distribution and the time difference between the inner low-resistivity 20-gap MRPC and the time reference PMTs (S1–S4) after correction is

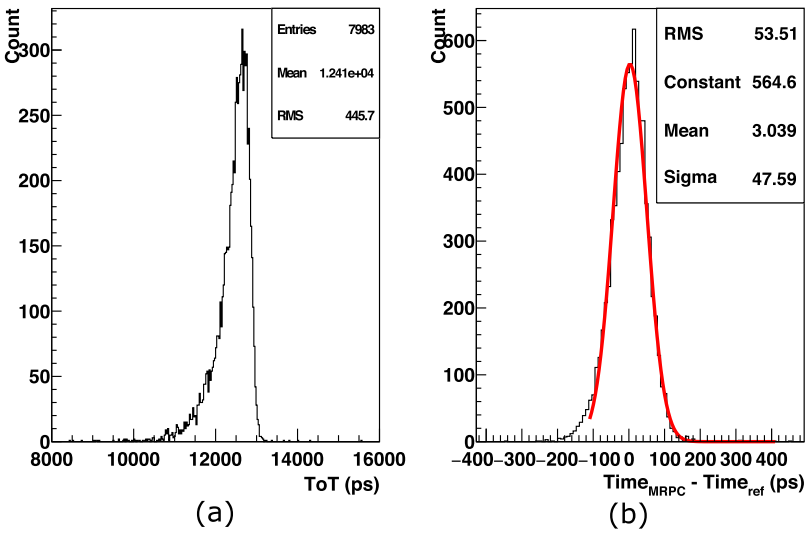

Fig. 6. (a) ToT distribution of the inner low-resistivity 20-gap MRPC. (b) Time difference between time reference PMTs (S1–S4) and the hits in the inner low-resistivity 20-gap MRPC after slewing corrections. The electric field of MRPC is 117.5 kV/cm.

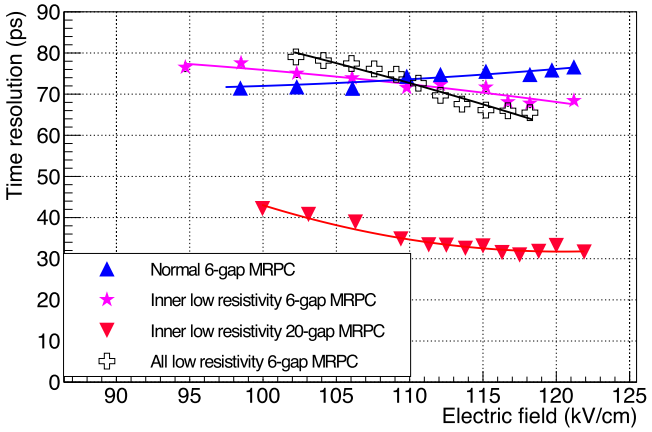

Fig. 7. The time resolution of the four MRPCs as a function at different electric fields at an instantaneous flux of 2.5 kHz/cm^2. The error bars are contained in the size of the symbols; the lines are just to guide the eye.

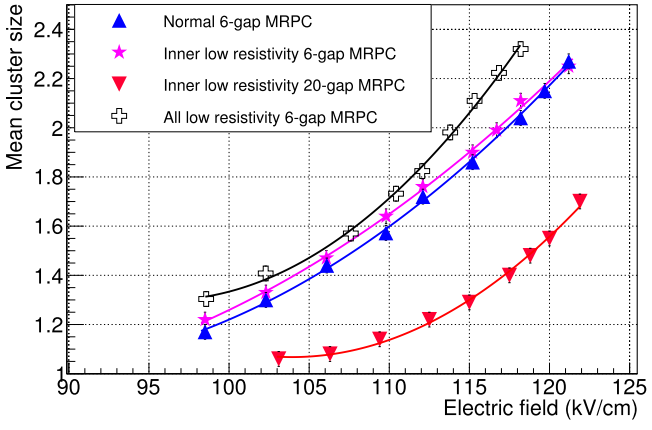

Fig. 8. Mean cluster size of the four MRPCs as a function at different electric fields at an instantaneous flux of 2.5 kHz/cm^2. The error bars are contained in the size of the symbols; the lines are just to guide the eye.

shown in Fig. 6. The time resolution of the inner low-resistivity 20-gap MRPC can be calculated as $\sqrt{47.6^2 - 35^2} = 32.3 \pm 1.2$ ps. Following this time-slewing correction technique, we obtained the time resolution of the four MRPCs at different electric field; this is shown in Fig. 7. The time resolution of MRPCs varies with applied electric fields. As the electric field increased from 94.7 kV/cm to 118.2 kV/cm, the time resolution of the normal 6-gap MRPC deteriorates from 70 ps to 75 ps. In contrast to the normal 6-gap MRPC, the time resolution of the inner low-resistivity 6-gap MRPC and all low-resistivity 6-gap MRPC improves with increasing electric field. As expected, the time resolution of the inner low-resistivity 20-gap MRPC is much better than that of the 6-gap MRPCs. As can be seen in Fig. 7, the time resolution of the inner low-resistivity 20-gap MRPC is below 35 ps from 111.3 kV/cm to 121.9 kV/cm.

The mean cluster size of the four MRPCs has also been measured. It is the average number of strips that fire for a through going particle and the result is shown in Fig. 8. The mean cluster size of the three 6-gap MRPC is quite similar (they have the same strip width). The mean cluster size of the inner low-resistivity 20-gap MRPC is lower than other 6-gap MRPCs and the main reason is it has a wider strip width.

The above results from these four MRPCs show that the MRPC using this low-resistive glass works well as resistive plate and gives good time resolution at low flux.

4.2. Flux scan of MRPCs

To check the rate capability of the MRPCs, the instantaneous flux of particles is varied between 2.5 kHz/cm^2 and 30.0 kHz/cm^2 for the normal 6-gap MRPC and the two inner low-resistivity MRPCs. For the all low-resistivity 6-gap MRPC, the instantaneous flux of particles has been increased to 90.0 kHz/cm^2, which is the maximum flux at T10.

The beam spill of 360 ms was divided into 10 slices offline. So each time bin is 36 ms, the estimated error for the slice time is 3 ms most. The efficiency of the four MRPCs for a given slice of the beam spill is plotted in Fig. 9. At the flux of 30 kHz/cm^2, the efficiency of all four MRPCs decreases during the spill. The efficiency of the normal 6-gap MRPC drops sharply at the beginning of the spill and flattens towards the end of the spill. Compared to the normal 6-gap MRPC, the efficiency of the other three MRPCs reduces much less. The efficiency of the all low-resistivity 6-gap MRPC becomes stable at the value of 94.8% in the last 100 ms at the flux of 30 kHz/cm^2.

In our analysis, to make our result match a continuous flux condition, we have used the data at the last 100 ms of the spill when the efficiency of MRPC is relatively stable. To compare the performance of

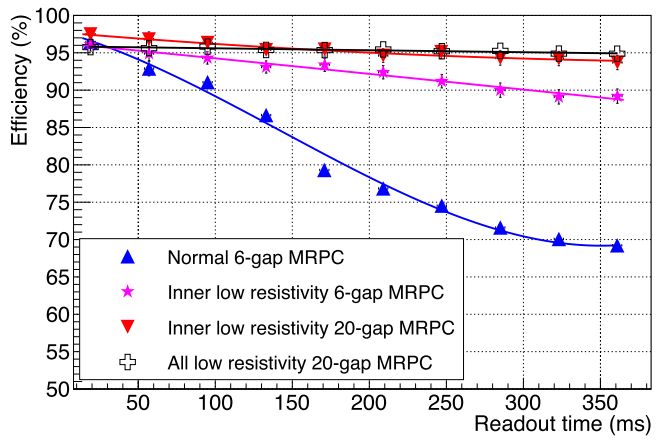

Fig. 9. The efficiency of the four MRPCs at an instantaneous flux of 30 kHz/cm^2 during 360 ms spill time. The error bars are contained in the size of the symbols; the lines are just to guide the eye.

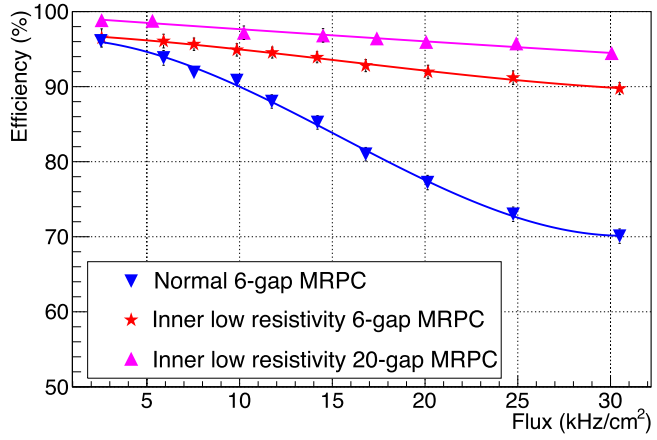

Fig. 10. The efficiency of the three MRPCs as a function of flux.

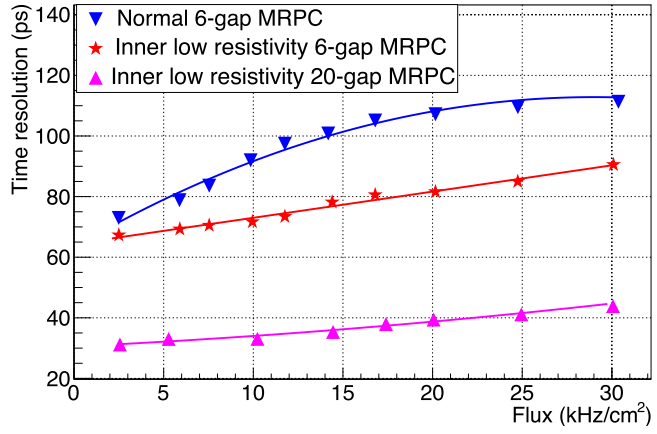

Fig. 11. The time resolution of the three MRPCs as a function at different flux.

the four MRPCs at high flux, the electric field of the three 6-gap MRPCs is fixed at 118.2 kV/cm (applied voltage of 15.6 kV across 6 gas gaps of 0.2 mm). The electric field of the inner low-resistivity 20-gap MRPC is 117.5 kV/cm. The efficiency and the time resolution of the four MRPCs at different flux are shown in Figs. 10–12. The efficiency of the normal 6-gap MRPC drops much faster than that of the other three MRPCs. At 30 kHz/cm^2, the efficiency of normal 6-gap MRPC has dropped to 70%. But the inner low-resistivity 6-gap MRPC and inner low-resistivity

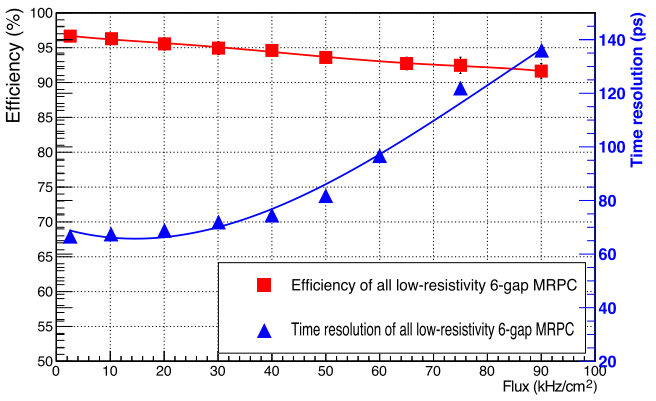

Fig. 12. The efficiency and time resolution of the all low-resistivity 6-gap MRPC as a function at different flux. The error bars are contained in the size of the symbols; the lines are just to guide the eye.

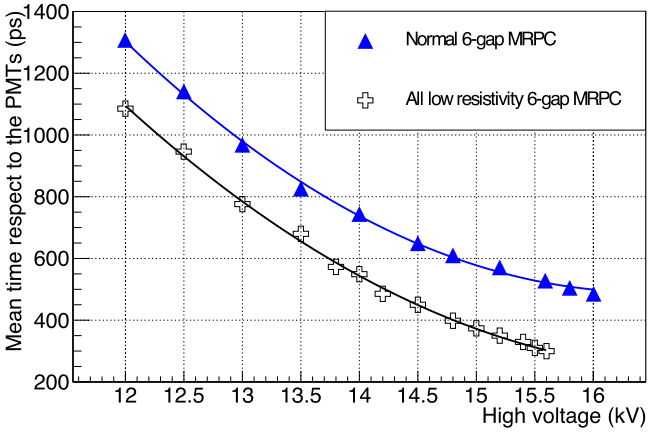

Fig. 13. The mean time of the normal 6-gap MRPC and the all low-resistivity 6-gap MRPC with respect to the PMTs (S1–S4) at different voltages at 2.5 kHz/cm^2. The error bars are contained in the size of the symbols; the lines are just to guide the eye.

20-gap MRPC still have an efficiency of 89% and 94%. The normal 6-gap MRPC has an 89% efficiency at the flux around 11 kHz/cm^2. This indicates that the inner low-resistivity 6-gap MRPC has an improvement of a factor 3 with rate capability by using low-resistive glass for inner plates. The time resolution of MRPCs deteriorates at higher flux. The normal 6-gap MRPC has significantly degraded timing performance at high flux. Its time resolution degrades from 72 ps to 114 ps from 2.5 kHz/cm^2 to 30.0 kHz/cm^2. The time resolution of the inner low-resistivity 6-gap MRPC degrades from 68 ps to 90 ps. The degradation of the inner low-resistivity 20-gap MRPC is much less than the other two MRPCs. At 30.0 kHz/cm^2, the time resolution is still 43 ps.

As can be seen from Fig. 12, the all low-resistivity 6-gap MRPC has been tested up to the flux of 90 kHz/cm^2. By using the low-resistive glass for all plates of this chamber, the rate capability is much higher than the normal 6-gap MRPC and has at least one order of magnitude improvement.

As the electric field is increased, the formation of the avalanche becomes earlier in time. We measure this shift in time as a function of applied voltage. This is shown in Fig. 13. When we operate the MRPC with a high flux we observe a shift in time during the beam spill (since there is a voltage drop across the resistive plates that leads to a reduction of the electric field in the gas gap). Thus, by measuring the time shift we can estimate the reduction of the electric field. For better comparison between this MRPC and the normal 6-gap MRPC, we estimate the voltage drop of these two MRPCs at different flux according to Fig. 13. The result is shown in Fig. 14. The voltage drop

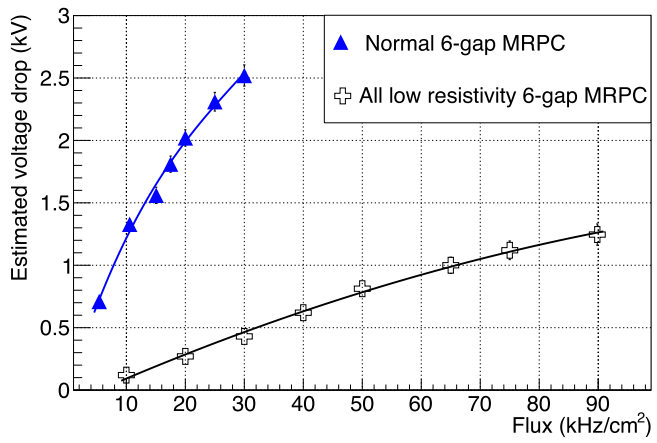

Fig. 14. The voltage drop of the normal 6-gap MRPC and the all low-resistivity 6-gap MRPC as a function of the flux. The error bars are contained in the size of the symbols; the lines are just to guide the eye.

of the normal 6-gap MRPC at 10.5 kHz/cm^2 is around 1.34 kV, which is larger than the 1.26 kV voltage drop of the all low-resistivity 6-gap MRPC at 90 kHz/cm^2. So the rate capability of this MRPC is at least one order of magnitude improved compared to the MRPC using only soda-lime float glass. However we expected a larger improvement, it could be related to the much smaller active area (5×6 cm^2) of the all low-resistivity MRPC, which is not much larger than the beam spot area as the normal 6-gap MRPC.

5. Discussion

The rate capability depends on the total resistance of a stack of glass plates. The normal 6-gap MRPC has 7 glass sheets of soda-lime float glass compared to the two soda-lime glass sheets of the inner low-resistivity 6-gap MRPC. We thus expect a rate capability of this inner 6-gap low-resistivity MRPC to be $7/2 = 3.5$ time higher. This is consistent with the results presented here. For the inner 20-gap low resistivity chamber; it has two high resistivity plates compared to the 11 plates of the MRPC presented previously [9]; we thus would expect a rate capability to improve by a factor 5.5. This number is also consistent. If the MRPCs were built only using low resistivity glass the improvement will be at least one order of magnitude; this has been confirmed by the result of all low-resistivity 6-gap MRPC. This indicates that this low-resistive glass can be used to construct the MRPC targeted for high flux experiments. These new low-resistivity glass sheets allow MRPCs to be built with many more gas gaps than using thicker material. Furthermore, the all low-resistivity 6-gap MRPC built with low-resistive glass sheets for the all plates reaches 96.5% efficiency and 66 ps time resolution at a low flux of 2.5 kHz/cm^2. It shows a high rate capability, which keeps 92% efficiency and 140 ps time resolution at an instantaneous flux of 90 kHz/cm^2. However, the result is a relative rate capability comparison between the MRPCs under a short pulsed beam with a small spot on the chamber. So there would be an overestimation of the working flux compared to a continuous full area irradiation.

Acknowledgements

The results presented here were obtained at the T10 test beam in the east hall at CERN. The authors acknowledge the support received by the operators of the PS.

References

[1] A.N. Akindinov, et al., Latest results on the performance of the multigap resistive plate chamber used for the ALICE TOF, Nucl. Instrum. Methods Phys. Res. A 533.1 (2004) 74–78.

[2] D. Belver, et al., The HADES RPC inner TOF wall, Nucl. Instrum. Methods Phys. Res. A 602 (2009) 687–690.

[3] B. Bonner, et al., A multigap resistive plate chamber prototype for time-of-flight for the STAR experiment at RHIC, Nucl. Instrum. Methods Phys. Res. A 478 (2002) 176–179.

[4] Johann M. Heuser, The compressed baryonic matter experiment at FAIR. EPJ Web of Conferences, vol. 13, EDP Sciences, 2011.

[5] I. Deppner, et al., The CBM time-of-flight wall: A conceptual design, J. Instrum. 9.10 (2014) C10014.

[6] D. Gonzalez-Diaz, et al., The effect of temperature on the rate capability of glass timing RPCs, Nucl. Instrum. Methods Phys. Res. A 555.1–2 (2005) 72–79.

[7] Jingbo. Wang, et al., Development of multi-gap resistive plate chambers with low-resistive silicate glass electrodes for operation at high particle fluxes and large transported charges, Nucl. Instrum. Methods Phys. Res. A 621.1–3 (2010) 151–156.

[8] A. Laso Garcia, et al., Extreme high-rate capable timing resistive plate chambers with ceramic electrodes, J. Instrum. 7.10 (2012) P10012.

[9] Z. Liu, et al., 20 gas gaps multigap resistive plate chamber: Improved rate capability with excellent time resolution, Nucl. Instrum. Methods Phys. Res. A 908 (2018) 383–387.

[10] http://sba.web.cern.ch/sba/BeamsAndAreas/East/East.htm.

[11] F. Anghinolfi, et al., NINO: An ultra-fast and low-power front-end amplifier/discriminator ASIC designed for the multigap resistive plate chamber, Nucl. Instrum. Methods Phys. Res. A 533 (1) (2004) 183–187.

[12] D. Breton, J. Maalmi, E. Delagnes, Using ultra fast analog memories for fast photo-detector read out, NDIP 2011, Lyon.